Development of a quantitative SRM-based proteomics method to study iron metabolism of Synechocystis sp PCC 6803

Vuorijoki, L.; Isojärvi, J.; Kallio, P.; Kouvonen, P.; Aro, E.M.; Corthals, G.L.; Jones, P.R.; Muth-Pawlak, D.

DOI
10.1021/acs.jproteome.5b00800

Publication date
2016

Document Version
Final published version

Published in
Journal of Proteome Research

Journal of proteome research

Article

pubs.acs.org/jpr

Development of a Quantitative SRM-Based Proteomics Method to Study Iron Metabolism of *Synechocystis* sp. PCC 6803

Linda Vuorijoki,[†] Janne Isojärvi,[†] Pauli Kallio,[†] Petri Kouvonen,[‡] Eva-Mari Aro,[†] Garry L. Corthals,[‡,§] Patrik R. Jones,[∥] and Dorota Muth-Pawlak*[,†,‡]

[†]Molecular Plant Biology, Department of Biochemistry, University of Turku, FI-20014 Turku, Finland

[‡]Turku Proteomics Facility, Centre for Biotechnology, University of Turku and Åbo Akademi University, FI-20014 Turku, Finland

[§]Van't Hoff Institute for Molecular Sciences, University of Amsterdam, 1018 WV Amsterdam, The Netherlands

[∥]Department of Life Sciences, Imperial College London, Sir Alexander Fleming Building, London SW7 2AZ, United Kingdom

Supporting Information

ABSTRACT: The cyanobacterium *Synechocystis* sp. PCC 6803 (*S.* 6803) is a well-established model species in oxygenic photosynthesis research and a potential host for biotechnological applications. Despite recent advances in genome sequencing and microarray techniques applied in systems biology, quantitative proteomics approaches with corresponding accuracy and depth are scarce for *S.* 6803. In this study, we developed a protocol to screen changes in the expression of 106 proteins representing central metabolic pathways in *S.* 6803 with a targeted mass spectrometry method, *selected* reaction *monitoring* (SRM). We evaluated the response to the exposure of both short- and long-term iron deprivation. The experimental setup enabled the relative quantification of 96 proteins, with 87 and 92 proteins showing adjusted *p*-values <0.01 under short- and long-term iron deficiency, respectively. The high sensitivity of the SRM method for *S.* 6803 was demonstrated by providing quantitative data for altogether 64 proteins that previously could not be detected with the classical data-dependent MS approach under similar conditions. This highlights the effectiveness of SRM for quantification and extends the analytical capability to low-abundance proteins in unfractionated samples of *S.* 6803. The SRM assays and other generated information are now publicly available via PASSEL and Panorama.

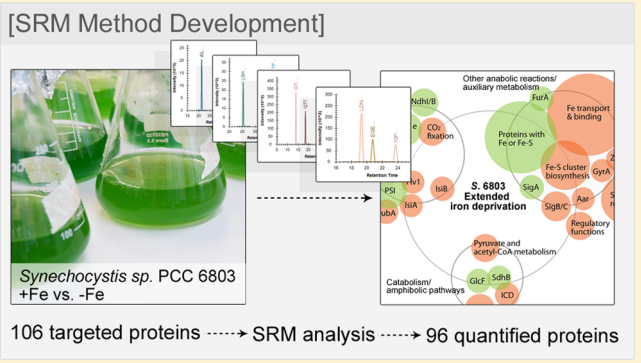

KEYWORDS: *selected reaction monitoring (SRM), quantitative proteomics, cyanobacteria, Synechocystis sp. PCC 6803, iron deprivation, metabolism*

INTRODUCTION

Cyanobacteria constitute a diverse group of oxygenic photosynthetic prokaryotes widely distributed in different habitats on Earth. They evolved water-splitting photosynthesis thus starting the oxygenation of the atmosphere, and they still carry a central role in global carbon and nitrogen cycling.[1] In principle, the evolution of cyanobacteria led to the evolution of chloroplasts in plants and algae, making cyanobacteria excellent model organisms to study the photosynthetic mechanisms and associated processes both at a molecular and systems level.

Out of the 2698 known cyanobacterial species,[2] *Synechocystis* sp. PCC 6803 (*S.* 6803 from hereon) is most extensively studied. Genomic and transcriptomic research has provided fundamental understanding on the underlying regulatory mechanisms of photosynthesis as well as the related cellular processes, in parallel to the development of tools and techniques for engineering the organism toward biotechnological applications.[3] These applications, such as those related to the design of more efficient bioenergy production platforms in *S.* 6803, are expected to promote the expansion of cost-effective clean technologies as part of sustainable bioeconomy. In order to stimulate further progress, new analytical methods are needed to obtain a more comprehensive and detailed view of the dynamic changes and complex interactions of proteins in the biological reaction network. Various proteomics techniques have been developed to characterize the proteome in systems biology studies and for efficient characterization of engineered systems *in vivo*.[4] However, consistent detection and precise quantification of proteins of interest across multiple samples and with high throughput remains as a general challenge for the current quantitative proteomics approaches, also those applied in studies with *S.* 6803.[5,6]

Despite advances in analytical techniques, protein quantification in complex biological samples is challenging and requires careful choice of quantitative approach. Two widely used protein quantification techniques in cyanobacteria are *difference gel electrophoresis* (DIGE) and *liquid chromatography mass*

Received: August 27, 2015
Published: December 10, 2015

DOI: 10.1021/acs.jproteome.5b00800
J. Proteome Res. 2016, 15, 266−279

spectrometry (LC-MS). In DIGE, the proteins are separated on a 2D gel and quantified based on fluorescence dyes.[7−9] The differentially expressed proteins can be further identified by mass spectrometry methods. The LC-MS techniques rely on data-dependent acquisition (DDA) and have the advantage to simultaneously identify and quantify even hundreds of proteins present in a sample. Label-based quantitative LC-MS techniques applied in the study of *S.* 6803 are based on chemical labeling that take advantage of modification of peptide sequence with the heavy labeled group as for example isobaric tags in TMT (Tandem Mass Tag)[10,11] and iTRAQ (isobaric Tags for Relative and Absolute Quantification)[12−14] or dimethylation approach.[15] Out of these methods, iTRAQ has been the most popular as it is well established and enables high throughput assays. Mass-spectrometry-based proteomics approaches can also be used for relative label free quantification, which rely on spectral counting[16,17] or peptide peak intensities.[18,19] The application of MS methods in *S.* 6803 proteome studies have been described in detail in a recent review by Battchikova et al. 2014.[20] The above-mentioned label and label-free approaches use untargeted DDA technique which is biased toward high-abundance proteins and suffer from inconsistent reproducibility in peptide detection in contrast to the targeted methods as SRM.[21,22] In DDA experiments, typically the most abundant precursor ions are automatically chosen for fragmentation and thus identified, rendering the less prominent signals from low abundant peptides more difficult to detect. Problems with the reproducibility may arise when different sets of peptide precursors are detected in different replicates. The proteome coverage of shotgun methods can be enhanced by sample fractionation and depletion of the most abundant proteins, which results in less complex samples with more peptide identifications and broader dynamic range.[23−25] In the label-free approach, however, fractionation may increase the technical variation, due to additional sample processing steps and thus is not the optimal method in high throughput studies.

The limitations associated with quantitative DDA proteomics can be partially overcome by applying a *selected* reaction *monitoring* (SRM) technique.[26] SRM is a targeted approach that allows precise and reproducible quantification of a predetermined set of proteins, however it requires a tedious method development. The specificity and sensitivity of the method is higher than in quantitative DDA proteomics due to the application of a triple quadruple (QQQ) mass spectrometer. The method measures selected precursor (Q1) to fragment ion (Q3) transitions which are derived from proteotypic peptides (PTPs)[27] used as protein surrogates. These parameters (mass to charge ratio m/z of precursor and fragment ions) together with retention time and spectral library information comprise the validated SRM assay. The strength of the SRM method is in its portability because once the SRM assay is established for a given protein, it can be applied in other laboratories on any triple quadruple instrument.[28] SRM can, in most cases, replace antibody-based quantification with similar specificity and sensitivity, but additionally, it can also provide high quality quantitative information at relatively high throughput.[29]

The SRM technique has recently been applied to yeast,[30] bacteria,[21,31] and human[32−34] samples but also to plants[35,36] and cyanobacteria,[37,38] although at much smaller scale. Toward the objective of generating targeted high-quality data sets for integrating systems biology and network analysis of *S.* 6803 metabolism, we aimed at establishing an SRM protocol for comprehensive monitoring of metabolic pathways and their interactions in *S.* 6803. The study was designed to reveal changes associated with iron deprivation, so proteins related to iron metabolism were particularly emphasized in our SRM target selection. In comparison to the shotgun proteomics techniques applied in *S.* 6803, the SRM-method was expected to allow precise quantification of also low-abundance proteins from unfractionated cell lysates. The driving force of this study was to develop a set of validated SRM-assays and provide this information in public repositories. This information could be easily retrieved and used by other scientists without tedious method development.

EXPERIMENTAL PROCEDURES

Growth Conditions

Synechocystis sp. PCC 6803 was grown in BG11 medium, pH 8.0, at +30 °C under a light intensity of approximately 50 μmol photons m^{-2} s^{-1} in an AlgaeTron230 incubator with agitation at 150 rpm in a 1% CO_2 environment. For the iron depletion study, cells were grown in BG11-medium in which $FeNH_4$-citrate was eliminated. The cell density was estimated by measuring the optical density at 750 nm ($OD_{750\ nm}$) with a Genesys 10S UV−vis spectrophotometer (Thermo Scientific).

The precultures were collected by centrifugation (4000*g* 10 min at room temperature) once $OD_{750\ nm}$ reached ∼1.0. Cells were washed twice either with iron sufficient or depleted BG11, depending of the future treatment, and centrifuged as previously described. The washed precultures were inoculated to 50 mL batches of respective growth media and the starting $OD_{750\ nm}$ was adjusted to ∼0.1. In order to remove all traces of iron from the culture flasks, the glassware were treated with 10% HCl (v/v) and 10 μM EDTA prior to autoclaving.

The cell growth was measured over time and the cells were harvested from both iron sufficient and deprived conditions, once the $OD_{750\ nm}$ reached 1.0 and after 12 days under iron deprivation. The growth patterns were verified by repeating the growth experiments several times.

Sample Preparation

Cells were collected by centrifugation at 8000*g* for 10 min at 4 °C and washed twice with 50 mM TES-KOH buffer, pH 8.0. The cell pellet was suspended in a protein extraction buffer (0.1% (w/v) RapiGest SF (Waters Corporation, Milford, MA) in 8 M urea solubilized in 0.1 M NH_4HCO_3 supplemented with 200 μM PMSF) together with an equal volume of acid washed glass beads (150−212 μm, Sigma). The cells were thereafter broken using a bead beater (Mini-Bead-Beater-8, Unigenetics Instruments Pvt. Ltd., India) with six cycles of 45 s shake with 3 min incubation on ice. Unbroken cells and glass beads were removed by centrifugation for 5 min at 1000*g* and again for 20 min at 12 000*g* at room temperature. The protein concentration was measured with the Bradford method (Bio-Rad). Proteins were reduced with 5 mM dithiotreitol (DTT, Sigma), alkylated with 10 mM iodoacetamide (IAA, Sigma) and precipitated with 1:5 v/v of 50% acetone/50% ethanol o/n at −20 °C. The pellet was centrifuged at 13 200 rpm at +4 °C for 30 min and solubilized by trypsin (Sequence grade Modified, Promega, Madison, WI, U.S.A.) digestion (1:100 trypsin:protein ratio) in 50 mM NH_4HCO_3 and 5% (v/v) acetonitrile (ACN) buffer for 4−5 h at +37 °C shaking. Digestion was continued for an additional 15−16 h following a second addition of trypsin in the same ratio. The digestion was stopped by adding formic acid (FA) (Sigma) to a final concentration of 0.5−1% (v/v) to

DOI: 10.1021/acs.jproteome.5b00800
J. Proteome Res. 2016, 15, 266−279

Table 1. Proteins Quantified in the SRM-Assay[a]

Gene ID	Gene name	Protein name	Function / metabolic context	log2 FC OD1	log2 FC 12d
Photosynthesis & Carbon fixation					
slr1329	atpD, atpB	ATP synthase beta subunit	ATP synthase	0.127	0.310
sll1525	prk, ptk	phosphoribulokinase	CO2 fixation	NQ	0.555
slr2094	fbpI, glpX	fructose-1,6-/sedoheptulose-1,7-bisphosphatase	CO2 fixation	0.336	0.697
sll1031	ccmM	carbon dioxide concentrating mechanism protein CcmM, putative carboxysome structural protein	CO2 fixation	0.707	0.586
sll1734	cupA, chpY	protein involved in low CO2-inducible, high affinity CO2 uptake	CO2 fixation	0.991	0.448
slr0009	rbcL	ribulose bisphosphate carboxylase large subunit	CO2 fixation	1.315	1.450
slr0342	petB	cytochrome b6 (MP)	Cytochrome b6/f complex*	-1.318	-1.570
sll1316	petC, petC1	cytochrome b6-f complex iron-sulfur subunit (Rieske iron sulfur protein) (MP)	Cytochrome b6/f complex*	-1.151	-1.265
sll0550	flv3	flavoprotein	Detoxification*	-1.103	0.490
sll1521	flv1	flavoprotein	Detoxification*	-0.634	1.197
sll0520	ndhI	NADH dehydrogenase subunit NdhI	NADH dehydrogenase*	-2.083	-1.694
sll0223	ndhB	NADH dehydrogenase subunit 2 (MP)	NADH dehydrogenase	-0.490	-0.798
slr1302	cupB, chpX	protein involved in constitutive low affinity CO2 uptake	Other	-0.458	0.117
slr0737	psaD	photosystem I subunit II	Photosystem I	-1.882	-3.671
slr1835	psaB, psaA	P700 apoprotein subunit Ib (MP)	Photosystem I*	-1.830	-3.548
ssl0563	psaC, psaC2	photosystem I subunit VII	Photosystem I*	-1.657	-3.298
sll0247	isiA, psbC	iron-stress chlorophyll-binding protein, homologous to psbC (CP43) (MP)	Photosystem I	11.332	12.117
sll1398	psb28, psb13, ycf79, psbW, psb28-1	photosystem II reaction center 13 kDa protein	Photosystem II	NQ	-0.272
sll0849	psbD1, psbD, psbD-1, psbDI	photosystem II reaction center D2 protein (MP)	Photosystem II*	-1.438	-2.076
ssr3451	psbE	cytochrome b559 alpha subunit (MP)	Photosystem II*	-1.063	-1.872
slr1311	psbA2, psba-2, psbA, psbAII	photosystem II D1 protein (MP)	Photosystem II*	-0.791	-1.711
sll0427	psbO	photosystem II manganese-stabilizing polypeptide (MP)	Photosystem II	-0.665	-1.506
slr1963	ocp	water-soluble carotenoid protein	Photosystem II	1.907	2.887
sll1578	cpcA	phycocyanin alpha subunit	Phycobilisome (PBS)	-0.843	-1.401
slr2067	apcA	allophycocyanin alpha subunit	Phycobilisome (PBS)	-0.716	-0.901
slr0335	apcE	Phycobilisome (PBS) core-membrane linker polypeptide	Phycobilisome (PBS)	-0.626	-0.724
slr2033	rubA	membrane-associated rubredoxin, essential for photosystem I assembly (MP)	PSI-biogenesis*	0.440	0.742
slr2082	ctaD, ctaII, ctaDII, cta2	cytochrome c oxidase subunit I (MP)	Respiratory terminal oxidases (RTO)*	0.270	0.659
sll0813	coxB, ctaC, ctaCII, cta2	cytochrome c oxidase subunit II (MP)	Respiratory terminal oxidases (RTO)	0.408	0.899
slr1379	cydA, cyd-1	quinol oxidase subunit I (MP)	Respiratory terminal oxidases (RTO)	0.459	1.421
sll0741	nifJ, Pfo	pyruvate flavodoxin oxidoreductase	Soluble electron carriers*	-3.729	-2.832
sll1382	petF, fdx, fedII, fdx II	ferredoxin, petF-like protein	Soluble electron carriers*	-2.160	-2.713
slr0150	petF, fdx, fdx IV	ferredoxin, petF-like protein	Soluble electron carriers*	-2.093	-1.958
slr1643	petH	ferredoxin-NADP oxidoreductase	Soluble electron carriers*	-0.122	NQ
ssl3044	-	probable ferredoxin, hydrogenase subunit	Soluble electron carriers*	NQ	0.392
sll0248	isiB, fla	flavodoxin	Soluble electron carriers	10.405	9.899
Other anabolic reactions/ auxiliary metabolism					
sll1356	glgP, glgY	glycogen phosphorylase	Carbohydrate metabolism*	0.512	1.489
sll0158	glgB	1,4-alpha-glucan branching enzyme	Carbohydrate metabolism	0.958	1.460
sll0169	zipN, ftn2	cell division protein Ftn2 homolog (MP)	Cell division	0.447	1.345
slr1516	sodB	superoxide dismutase	Detoxification*	-2.014	-2.704
slr0417	gyrA	DNA gyrase subunit A	DNA unwinding	0.760	1.020
sll0698	hik33, chk33, ycf26, dspA, nblS, dfr	drug sensory protein A, low temperature sensor, two-component sensor histidine kinase (MP)	Drug and analog sensitivity	0.341	0.370
slr1511	fabH	3-oxoacyl-[acyl-carrier-protein] synthase III	FA-biosynthesis	0.462	0.339
sll0728	accA	acetyl-CoA carboxylase alpha subunit	FA-biosynthesis	0.518	0.146
slr1890	bfrB	bacterioferritin	Fe-transport and binding*	-0.349	0.194
sll1341	bfrA	bacterioferritin	Fe-transport and binding*	NQ	0.720
slr0327	futB, hitB	iron(III) ABC transporter, permease protein (MP)	Fe-transport and binding	2.302	2.640
sll1878	futC	iron(III)-transport ATP-binding protein	Fe-transport and binding	3.981	4.033
slr0513	futA2, idiA, futA	iron transport system substrate-binding protein, periplasmic protein	Fe-transport and binding*	4.619	5.107
slr1295	futA1, sufA, sufA1, idiA, futA	iron transport system substrate-binding protein	Fe-transport and binding*	4.819	4.989
slr1392	feoB	ferrous iron transport protein B (MP)	Fe-transport and binding*	5.750	5.364
sll1406	fhuA	ferrichrome-iron receptor (MP)	Fe-transport and binding*	9.563	9.431
sll1454	narB	ferredoxin-nitrate reductase	Glutamate family / Nitrogen assimilation*	-1.099	-1.455
sll0208	ado	aldehyde deformylating oxygenase	Hydrocarbon biosynthesis*	NQ	NQ
sll0209	aar	Acyl-ACP reductase	Hydrocarbon biosynthesis	0.676	0.894
sll1221	hoxF	diaphorase subunit of the bidirectional hydrogenase	Hydrogenase*	-3.028	-2.609
sll1223	hoxU	diaphorase subunit of the bidirectional hydrogenase	Hydrogenase*	-2.581	-1.971
sll1226	hoxH	hydrogenase subunit of the bidirectional hydrogenase	Hydrogenase*	-0.286	-0.610
slr1417	ycf57, iscA, sufA, iscA1	hypothetical protein YCF57 (MP)	Iron-sulphur cluster biosynthesis*	NQ	0.252
slr0075	ycf16, sufC	ABC transporter ATP-binding protein	Iron-sulphur cluster biosynthesis	0.169	0.440
slr0077	sufS, nifS	cysteine desulfurase	Iron-sulphur cluster biosynthesis	0.358	0.664
slr0074	ycf24, sufB	ABC transporter subunit	Iron-sulphur cluster biosynthesis	0.451	0.574
slr0076	sufD, sufB	hypothetical protein	Iron-sulphur cluster biosynthesis	0.512	0.629
slr2143	cefD	L-cysteine/cystine lyase	Iron-sulphur cluster biosynthesis	0.774	1.758
slr0387	nifS1, iscS	cysteine desulfurase NifS	Iron-sulphur cluster biosynthesis	1.129	2.264
sll0088	sufR	hypothetical protein	Iron-sulphur cluster biosynthesis*	2.075	2.465
slr1239	pntA	pyridine nucleotide transhydrogenase alpha subunit (MP)	NAD(P)-metabolism	0.112	0.516
slr1894	mrgA	probable DNA-binding stress protein	Nucleoproteins*	1.045	2.151
sll0567	fur, furA	ferric uptake regulation protein	Regulatory functions*	-2.458	-1.271
sll1626	lexA	LexA repressor	Regulatory functions	0.385	0.982
sll1423	ntcA, ycf28	global nitrogen regulator	Regulatory functions	0.522	1.494
slr0653	sigA, rpoDI, rpoD1, cax, rpo	principal RNA polymerase sigma factor SigA	RNA synthesis, modification, and DNA transcription	-0.348	-0.759
ssl2982	ycf61	probable DNA-directed RNA polymerase omega subunit	RNA synthesis, modification, and DNA transcription	0.145	NQ
sll0184	rpoD, sigC	group2 RNA polymerase sigma factor SigC	RNA synthesis, modification, and DNA transcription	0.975	1.538
sll0306	rpoD, sigB, sigB2	RNA polymerase group 2 sigma factor	RNA synthesis, modification, and DNA transcription	1.357	1.671
slr0963	sir	ferredoxin-sulfite reductase	Serine family / Sulfur assimilation*	0.289	0.384
sll0662	fed7	4Fe-4S type iron-sulfur protein	Soluble electron carriers*	-1.477	-1.775
slr0148	fdx	hypothetical protein	Soluble electron carriers*	-0.815	-0.940
sll1057	trx, trxM2, TrxZ, trxC	thioredoxin M	SS-bond reduction	NQ	NQ
slr0623	trxA, trxA1, trxM	thioredoxin	SS-bond reduction	0.249	1.129
slr1139	trx, trxA, trxA2, TrxX, trxB	thioredoxin	SS-bond reduction	0.444	1.190
sll1621	type II prx, aphC, PrxII, ahpC, sodB, type II prx	AhpC/TSA family protein	SS-bond reduction	0.806	0.911
slr1562	grxC, grx, grxB, grx1	glutaredoxin	SS-bond reduction	0.924	1.376
slr0600	NTR, trxR	NADP-thioredoxin reductase (MP)	SS-bond reduction	0.979	1.677
slr0348	lspH, lytB	hypothetical protein	Terpenoid/isoprene biosynthesis*	NQ	0.937
slr2136	gcpE	GcpE protein homolog	Terpenoid/isoprene biosynthesis*	0.175	0.351
Catabolism/ amphibolic pathways					
sll1831	glcF	glycolate oxidase subunit, (Fe-S)protein	Glycolate pathway*	-2.958	-1.153
sll1196	pfkA, pfkB1	phosphofructokinase	Glycolysis	0.282	0.574
slr1843	zwf	glucose 6-phosphate dehydrogenase	Pentose phosphate pathway	0.990	1.862
sll0329	gnd	6-phosphogluconate dehydrogenase	Pentose phosphate pathway	1.410	1.907
sll0542	acs	acetyl-coenzyme A synthetase	Pyruvate and acetyl-CoA metabolism	NQ	0.238
sll0920	ppc	phosphoenolpyruvate carboxylase	Pyruvate and acetyl-CoA metabolism	0.938	1.949
sll0823	sdhB	probable succinate dehydrogenase iron-sulfur protein	TCA cycle*	-2.135	-1.639
slr0665	acnB	aconitate hydratase	TCA cycle*	-1.923	-0.532
sll1625	sdhB	succinate dehydrogenase iron- sulphur protein subunit	TCA cycle*	-1.390	-0.428
slr1289	icd, icdA	isocitrate dehydrogenase (NADP+)	TCA cycle	0.698	1.531
Not detected in our experimental setup					
Gene ID	**Gene name**	**Protein name**	**Function / Metabolic context**		
Photosynthesis & Carbon fixation					
slr0040	cmpA	bicarbonate transport system substrate-binding protein	CO2 fixation		
slr0331	ndhD1	NADH dehydrogenase subunit 4 (involved in photosystem-1 cyclic electron flow) (MP)	NADH dehydrogenase		
sll0219	flv2	flavoprotein	Photosystem II*		
sll0217	flv4	flavoprotein	Photosystem II*		
slr0846	-	transcriptional regulator for psaAB	Regulatory functions		
Other anabolic reactions/ auxiliary metabolism					
slr0749	chlL	light-independent protochlorophyllide reductase iron protein subunit ChlL	Cobalamin, heme, phycobilin and porphyrin*		
sll0704	nifS	cysteine desulfurase	Glutamate family / Nitrogen assimilation		
slr1529	ntrX	nitrogen assimilation regulatory protein (MP)	Glutamate family / Nitrogen assimilation*		
slr1738	perR	transcription regulator Fur family	Regulatory functions		
ssl0564	pedR	transcriptional regulator	Regulatory functions		

[a]Gene symbols and names are based on Kasuza CyanoBase. Genes without respective symbols in CyanoBase are named after the literature. Protein upregulation and downregulation are shown in green and red gradient, respectively. The proteins which are differentially expressed in comparison to Wegener et al. 2010 are highlighted in red font. The 64 proteins not seen in shotgun by Wegener et al. are shown with a gray background. Proteins, which are predicted to be transmembrane proteins by TMHMM Server v. 2.0 are marked as (MP = membrane protein) in the Protein Name column. Presented are only the expression fold changes with p-value <0.01. Proteins which were regulated with p-values >0.01 are marked as NQ (Not Qualified). The proteins marked with asterisk (*) in the Function/metabolic context – column harbour Fe or Fe–S – binding motifs based on UniProt and Cyanobase annotations supplemented with literature search.

DOI: 10.1021/acs.jproteome.5b00800
J. Proteome Res. 2016, 15, 266–279

lower the pH below 2. The digestion mixture was incubated for 30 min at +37 °C at 130 rpm, and the water immiscible RapiGest SF degradation products were removed by centrifugation. To desalt the samples, solid phase extraction (SPE) of the peptide mixture was performed with a 4 mm/1 mL extraction disk cartridge (Empore C18-SD, 3M) according to manufacturer's protocol. The eluted peptide samples were vacuum-dried (Savant SPD1010, SpeedVac Concentrator, Thermo Scientific) and solubilized in 0.1% (v/v) FA and 2% (v/v) ACN and stored at −80 °C prior to MS analysis. The synthetic peptides were combined to one aliquot and desalted with the same protocol as above.

In vivo Absorption Spectra

In vivo absorption spectra were measured with an Infinite 200 PRO multiplate reader (Tecan) from 400 to 750 nm to monitor the development of iron deprivation in the cells by the characteristic shift in chlorophyll *a* absorbance.[39]

Selection of the Target Proteins

Altogether 106 proteins were selected to represent different metabolic pathways in *S.* 6803 in order to monitor the metabolic changes as broadly as possible, especially during iron deprivation. The targets were divided into three main categories: (1) photosynthesis and carbon fixation, (2) other anabolic reactions/auxiliary metabolism, and (3) catabolism/amphibolic pathways. These were further divided into altogether 35 subcategories described by the different functions (Table 1).

Design of the SRM Assay

The establishment of the SRM assay can be divided into three steps: (I) identification of proteins of interest, (II) the selection of PTPs representing the target proteins, and (III) the most intense transitions. Throughout the SRM-assay design (Figure 1), the open source software Skyline[40] was used. The background proteome for Skyline operations was built from FASTA files containing amino acid sequences from Cyanobase.[41]

Protein Identification - LC-MS/MS Analysis

Identification of the target proteins by a shotgun approach from unfractionated cell lysates of *S.* 6803 was performed on a nanoflow HPLC system (EasyNanoLC 1000, Thermo Fisher Scientific) coupled to the Orbitrap Velos Pro (Thermo Scientific) or Q Exactive (Thermo Scientific) mass spectrometer equipped with a nanoelectrospray ionization source. The peptides (250 ng/5 μL injection volume) were first loaded on a trapping column and subsequently separated in line on a 15 cm C18 column (75 μm × 15 cm, Magic 5 μm 200 Å C_{18}, Michrom BioResources Inc., Sacramento, CA, U.S.A.). The mobile phase consisted of water/ACN (98:2 (v/v)) with 0.2% FA (v/v) (solvent A) or ACN/water (95:5 (v/v)) with 0.2% FA (v/v) (solvent B). To elute peptides, 110 min gradient was used by increasing the solvent B ratio from 5% to 20% in 70 min following an increase to 40% in 30 min with the flow of 300 nL/min.

Data-Dependent Acquisition (DDA) Settings

DDA was performed on two types of mass spectrometers Orbitrap Velos Pro and Q Exactive. MS data was acquired automatically in positive ionization mode with 2.3 kV ionization potential using Thermo Xcalibur software (Thermo Fisher Scientific) in both instruments. The acquisition method consisted of an MS survey scan in the mass range of 300–2000 m/z. Up to 10 or 15 of the most intensive peaks from the full scan, with charge +2 and +3, were selected for HCD (high-energy collision dissociation) or CID (collison-induced

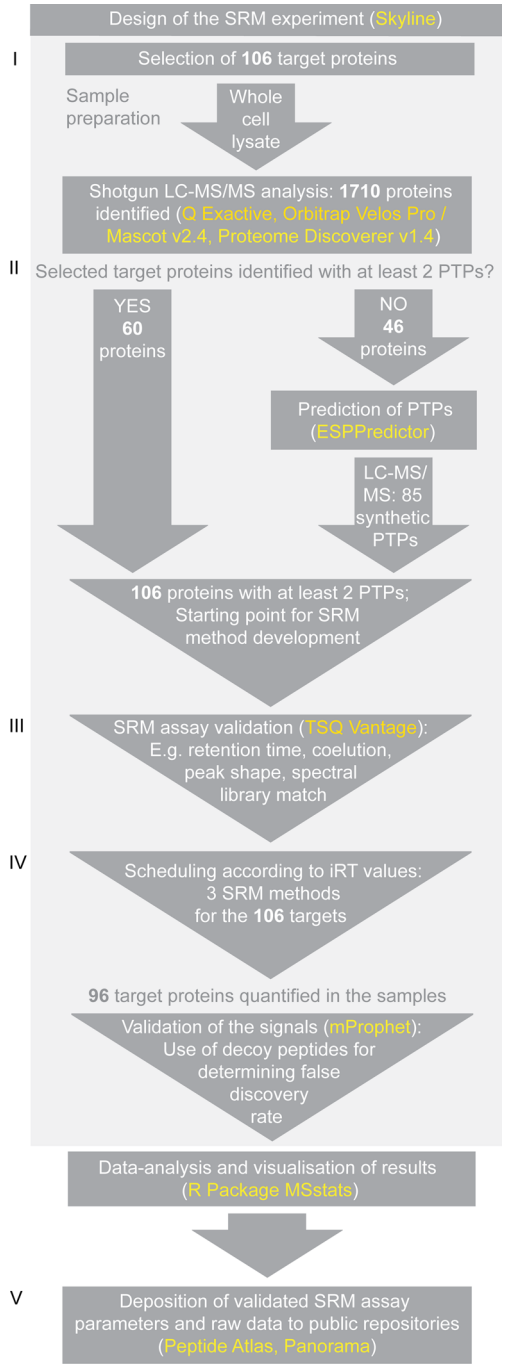

Figure 1. Workflow of the SRM assays development and validation for 106 proteins in *Synechocystis* sp. PCC 6803: (I) Selection of the proteins of interest, (II) identification of the proteotypic peptides for each target, (III) determination of the associated peptide transitions, (IV) setup of the SRM method and data-analysis, and (V) deposition of the final SRM assay parameters and data in publicly available databases. The equipment and software used in the study have been highlighted in orange and yellow, respectively.

DOI: 10.1021/acs.jproteome.5b00800
J. Proteome Res. 2016, 15, 266–279

dissociation) fragmentation in Q Exactive and Orbitrap Velos Pro, respectively. On Q Exactive the spectra were registered with a resolution of 70 000 and 17 500 (at m/z 200) for full scan and for fragment ions, respectively, and normalized collision energy of 27%. The AGC (automatic gain control) was set to a maximum fill time of 120 and 250 ms and to obtain maximum number of 1e6 and 2e4 ions for MS and MS/MS scans, respectively. On Orbitrap Velos Pro the MS1 spectra were registered with a resolution of 60 000. The AGC settings were set to a maximum fill time of 500 ms and maximum number of ions of 1×10^6 for MS and 200 ms and 5×10^3 for MS/MS scans. Normalized collision energy of 35% was applied.

DDA Data-Analysis

The raw data from the shotgun experiments performed by the two different mass spectrometers was searched against the *S.* 6803 protein database retrieved from Cyanobase[41] (3672 entries, 23.10.2012) using an in-house Mascot (v.2.4) search engine[42] and further analyzed using Proteome Discoverer (v.1.4) Software (Thermo Scientific). The following Mascot search parameters were used: trypsin as an enzyme, methionine oxidation as variable modification, and carbamidomethylation as fixed. The precursor value was restricted to monoisotopic with a mass tolerance of ±4 ppm (Q Exactive) or ±10 ppm (Orbitrap Velos Pro) and fragment ion mass tolerance of ±0.02 Da (Q Exactive) or ±0.8 Da (Orbitrap Velos Pro). Two missed cleavages were allowed and decoy searches were performed. For the validation of peptide identifications, the Percolator algorithm[43] (v 2.04, build date 01.02.2012) was used with minimum false discovery rate (FDR) of 0.05. The resulting msf-files were thereafter used to create MS/MS spectral libraries in Skyline.

Selection of PTPs for Target Proteins

In order to generate the SRM-assay, up to five PTPs per protein were selected which are unique for each target protein and give the most intense MS-signals. The criteria for the targeted peptides were defined in Skyline based on several physicochemical properties, which make the peptides most likely to be consistently observed in MS-runs. Only the unique peptides with +2 or +3 charge states and length of six to 25 amino acids without ragged ends (kk/rr/kr/rk) and missed cleavage sites for trypsin were allowed. Furthermore, methionine and sites prone to glycosylation (NXS/NXT) were avoided.

For the target proteins, which were not detected in data-dependent LC-MS/MS runs or did not have enough identified PTPs fulfilling the criteria set in Skyline, synthetic peptides were used (PepOtec Immuno Custom Peptide Library Service, Thermo Scientific). The missing PTPs were selected in Skyline and their potential detectability in MS was evaluated with the help of three different computational tools, ESPPredictor,[44] Peptide Sieve[45] and Peptide Detectability Predictor.[46] Out of the available tools, ESPPredictor was prioritized due to easy implementation. The other prediction tools were mainly used to confirm the peptide selections retrieved from ESPPredictor.

Selection of Transitions

The precursor to fragment ion transitions list was built based on spectral libraries created from the DDA database search results. Up to five of the most intense y-ions with mass-to-charge (m/z) ratios higher than the precursor were prioritized.

Retention Time Prediction

To enhance the multiplexing of the SRM assay and accuracy of the peptide retention time prediction, two different approaches were used. In the first step, SSRCalc 3.0 calculator[47] implemented in Skyline was applied to predict retention time for targeted peptides. To calibrate SSRCalc the unscheduled run was performed with carbonic anhydrase proteolytic peptides spiked in a *S.* 6803 pooled sample. With the obtained retention time values and calculated peptide hydrophobicity factors, the retention times for targeted peptides were estimated. In the second step, iRT kit[48] was used to enhance the accuracy of retention time assessment. On the basis of the calibration curve created for 11 standard iRT peptides according to manufacturer's instructions (Biognosys AG, Switzerland), the indexed retention time value for each of 375 target peptides was determined. The retention times measured for the iRT-standard peptides in the initial alignment run (Figure S-3), allows calculating the retention time for each peptide with associated iRT value (Figure 2b; iRT values for all targets listed in Supporting Table S-1).

SRM Analysis

The final list comprised 375 target peptides, which were randomly distributed to three different methods with 5 min retention time window ensuring minimum number of coeluting

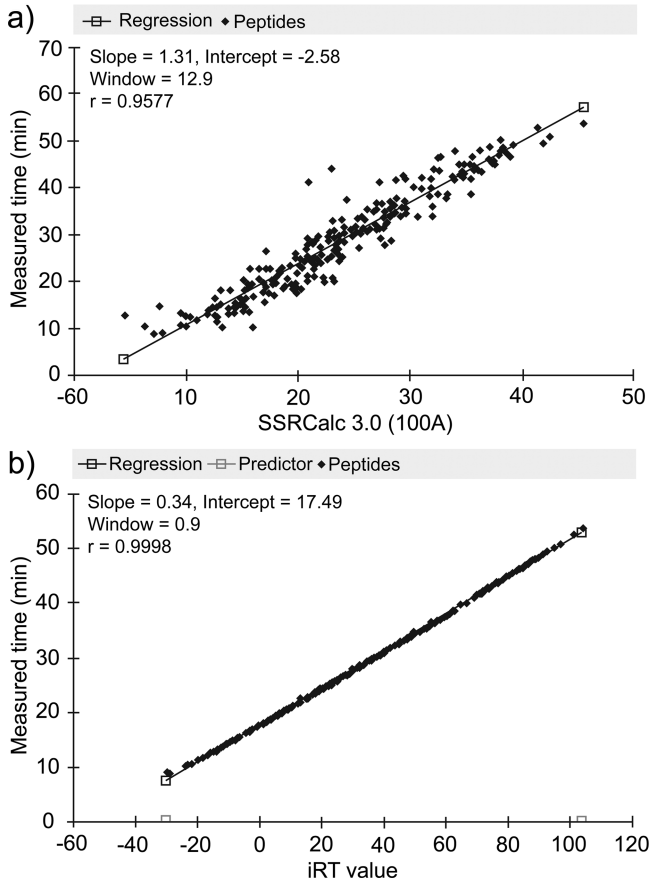

Figure 2. Comparison between the two calculators used in peptide retention time estimation. (a) The SSRCalc 3.0 retention time calculator allowed us to detect most of the targeted peptides in a 60 min LC-gradient. However, the use of (b) iRT calculator clearly increased the accuracy of retention time estimation for the target peptides (r = 0.9998) in comparison to SSRCalc 3.0 (r = 0.9577).

DOI: 10.1021/acs.jproteome.5b00800
J. Proteome Res. 2016, 15, 266−279

transitions. In each method, two stable endogenous standard peptides were included in order to normalize the run specific signal variations, and measurement errors and 11 iRT-standard peptides (Biognosys AG) were measured to ensure the stability of the scheduling.

The 126 decoys were generated by reversing the sequences of the randomly selected target peptides with the exception of C-terminal lysine or arginine (K or R) and measured. The m/z values of the precursor ions were changed for each decoy peptide. The iRT values for the decoys were the same as for the target peptides from which they were generated. The use of peptide decoys was necessary for calculating the false discovery rates (FDR, q-value) in mProphet.[49]

LC-QQQ-Settings

The samples were analyzed on a triple quadrupole mass spectrometer (TSQ Vantage, Thermo Scientific, San Jose, CA) equipped with nanoelectrospray source. The chromatographic separation of peptides was performed using a nanoflow HPLC system EasyNanoLC 1000 (Thermo Scientific). First, the samples were loaded into the trapping column (75 μm × 2 cm, 3 μm 120 Å C18, Reprosil-Pur, Dr. Maisch GmbH, Germany) after which the peptides were separated in an analytical column (75 μm × 15 cm, 3 μm 120 Å C18, Reprosil-Pur, Dr.Maisch GmbH, Germany) using a 50 min nonlinear gradient at a flow rate of 300 nL/min (5−20% B in 35 min; 20−35% B in 50 min; B = ACN:water, 98:5).

The mass spectrometer was operating in SRM − mode by applying 1600 V spray voltage, 270 °C capillary temperature, collision gas pressure of 1.2 mTorr argon in Q2 and tuned S-lens value. The Q1 and Q3 peak width was set to 0.7 unit resolution (fwhm), the cycle time was set to 2.5 s and the isolation width was 0.002 m/z. The SRM data was acquired by using the predicted, default collision energy (CE) values obtained from Skyline. The retention time window was set to 5 min and the dwell time 20 ms (min). For all samples, biological triplicates were measured.

SRM Data Analysis

Data-analysis was divided in two parts: peak picking and quantification. The first part was carried out in Skyline with mProphet algorithm which after training of the statistical model allows automatic peak identification. The obtained parameters were used to evaluate the confidence and significance of the data as false discovery rates and p-values (referring to *adjusted* p-values throughout the text) for each detected target peptide in each respective sample and condition (Figure 3). The relative quantification was done with the R package MSstats (version: 2.6.0).[50,51] The main considerations for the applied statistical model for the analysis were (1) the determination of the normalization method, (2) the scope of validity of the conclusions and, (3) the experimental design. The global standard normalization was used with two endogenous peptides (SNLDSNHIIYR and SEELLGAASNR). The relatively low amount of biological replicates determined the scope of conclusions to be restricted and thus valid only to the selected subjects (i.e., to the three replicates). The experimental design was based on MSstats implemented Group Comparison tool, which uses linear mixed models to test the protein abundances for significant changes across different conditions. Significance of the expression level change was evaluated for the acquired data with MSstats designSampleSize tool to establish a cut off fold change (FC) value which is statistically valid. The MSstats input file and R-script can be found from Supporting Information (Supporting Table S-2, MSstatsInput and R-code).

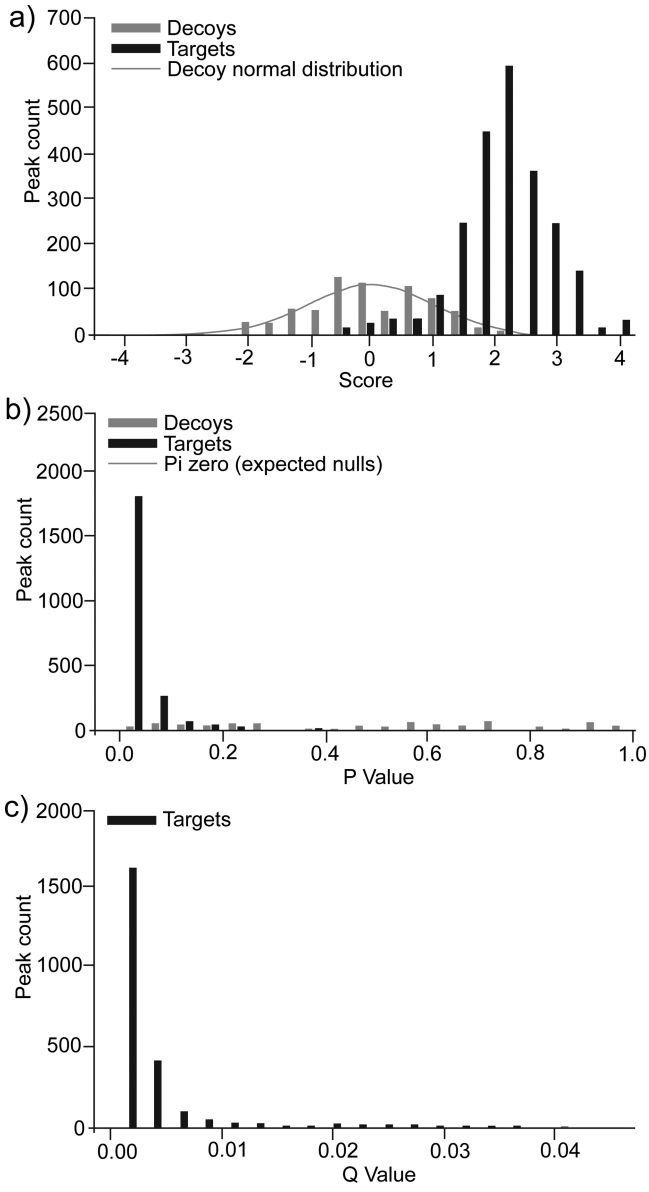

Figure 3. mProphet peak scoring model applied to the SRM data set for quality assessment. Represented are (a) composite score, (b) p-values, and (c) q-values for evaluation of the SRM data set against the targeted decoy peptides.

RESULTS

Selection of the Target Proteins

Altogether 106 target proteins were selected to represent key proteins in the metabolic network of *S.* 6803. These were divided into three main categories: (1) photosynthesis (41 proteins), (2) other anabolic reactions/auxiliary metabolism (55 proteins), and (3) catabolic/amphibolic pathways (10 proteins). The case study focused on elucidating the metabolic effects of iron deprivation, thus special emphasis was placed on the proteins related to iron metabolism; iron transport and storage, iron−sulfur cluster biogenesis, and associated proteins. The complete list of annotated targets is presented in Table 1. The proteins marked with an asterisk (*) harbor iron or iron−

DOI: 10.1021/acs.jproteome.5b00800
J. Proteome Res. 2016, 15, 266−279

sulfur binding motifs based on UniProt and Cyanobase annotations and a literature search.

SRM-Assay Establishment for the 106 Target Proteins

Protein Identification by DDA. The overall design of the SRM method for *S.* 6803 is illustrated in Figure 1. Initially, the target strain was cultivated under the specified conditions, and the extracted and digested samples were subjected to shotgun LC-MS/MS analysis. The obtained data was searched against the *S.* 6803 proteome database and the combined results led to identification of altogether 1710 proteins, represented in total by 15 031 unique peptides (46% coverage of the *S.* 6803 proteome) (Supporting Table S-3). The preliminary analysis was performed with Orbitrap Velos Pro while the following runs were carried out with Q Exactive using similar fragmentation mode (HCD) as QQQ which was considered beneficial. Moreover, the spiked-in synthetic peptides were analyzed only by Q Exactive, which further increased the achieved coverage. The use of two different instruments for obtaining the data resulted in separate spectral libraries with complementary sets of peptides. Thus, the rationale for exploiting the two instruments was not to compare their performance but to provide a comprehensive data set, which could be used for designing the method in Skyline. The spectra obtained with HCD fragmentation type were favored because it provides the fragmentation pattern that correlates better with the intensities obtained in QQQ instrument.[52] So far, there is no open data repository for spectral library information for *S.* 6803, and the libraries generated here provided the first template for the design of any further SRM assays in this cyanobacterial model species. The spectral library data set is accessible via Panorama[53] (Supporting Information; https://panoramaweb.org/labkey/Vuorijoki_et_al_2015.url).

Out of the 106 target proteins listed in Table 1, 60 were identified in the initial LC-MS/MS analysis, each with at least two endogenous PTPs. The remaining 46 targets represented proteins which are typically challenging to find in the DDA approach from unfractionated samples due to their low relative abundance or differential detectability of the proteolytic peptides. Although for some of these proteins, there were two or more detected PTPs in the shotgun experiments, the fragmentation spectrum was not adequate in providing reliable information for SRM assays. To allow reliable identification and quantification of these proteins, 85 PTPs were selected with computational peptide prediction tools and synthesized (PepOtec Immuno Custom Peptide Library Service, Thermo Scientific) to obtain sufficient amount of quantifiable PTPs for each protein (Supporting Table S-1). Subsequent analysis of the synthetic peptides by LC-MS/MS allowed us to increase the number of quantifiable targets up to 106 and to expand the SRM method to also cover the low-abundance proteins.

Determination of SRM Assay Parameters. Several parameters were considered in the process of SRM assay development: choice of the most abundant PTPs, most intense and thus most sensitive precursor to fragment ion transitions, similarity between relative intensities in reference spectrum and SRM traces (dot value >0.8), and retention time of targets in correlation with SSRCalc or iRT calibration curve ($r > 0.9$) (Figure 2). The pooled sample, containing both endogenous and synthetic peptides, was subjected to scheduled SRM analysis in order to verify the information retrieved from spectral libraries generated in DDA. Initially the retention times were estimated based on calibration run using the SSRCalc calculator[47] implemented in Skyline in order to minimize the number of analytical runs. Most of the targeted peptides could be found in the predicted retention time window with a correlation of $r = 0.9577$ between the predicted and experimental retention times (Figure 2a). For the remaining targets, the unscheduled SRM run was performed. To enhance the accuracy of the retention time estimation for the future experiments, iRT-standard peptides[48] were introduced for determining iRT values for each target peptide. This resulted in an increased accuracy in retention time estimation with a correlation of $r = 0.9998$ (Figure 2b). It is important to point out that the triple quadrupole instrument can analyze only a limited number of transitions at a time, and therefore, there is a need for precise scheduling in order to increase the multiplexity of the SRM-method and maximize its accuracy and sensitivity. The iRT values provided here can be used to calculate the retention time of any of the studied peptides in any other LC-MS system at the expense of only one alignment run with iRT standards.

The entire procedure allowed us to set up an SRM protocol for *S.* 6803 with validated peptide transitions for 106 different proteins. The obtained SRM parameters were tested in real biological samples, and majority of the interferences were excluded from the analysis upon quality assessment carried out with mProphet algorithm, while the remaining ones had negligible effect on the data. The final assay parameters are presented in the Skyline file published in Panorama Public (Supporting Information).

Application of SRM To Study the Effect of Iron Deprivation. As a first case study, the established SRM protocol was used to study the effects of iron deprivation on *S.* 6803 metabolism in order to further evaluate and compare the method to previously used proteomics approaches. A quantitative analysis was carried out without spiked-in synthetic peptides to compare iron sufficient and iron deprived batch cultivations harvested at $OD_{750\ nm}$ ~1 and after 12 days under iron deprivation (Figure S-1 and S-2; growth curves and absorption spectra). Out of the 106 target proteins in the SRM protocol, 96 proteins were successfully quantified in the analysis with average coefficient of variation (CV) for all experiment of 10% (Supporting Table S-4, Supporting Figure S-4). The remaining 10 undetected proteins were either not expressed under the experimental conditions (sll0219 and sll0217),[54] or were present in very low quantities, possibly due to poor recovery during sample processing as often is the case with the integral membrane proteins (slr0331 and slr1529).[55] Skyline files with the results and the raw data with the transition list are available from Panorama (https://panoramaweb.org/labkey/Vuorijoki_et_al_2015.url) and PASSEL[56] with PASS00726 identifier (https://db.systemsbiology.net/sbeams/cgi/PeptideAtlas/PASS_View), respectively.

Throughout data-analysis, the statistically significant changes in protein expression levels were set to have *p*-values less than 0.01. The proteins with higher *p*-values (*p*-value >0.01) showed negligible expression level changes and are listed as part of the Supporting Tables S-5 and S-6. The significance of the expression level change was estimated with MSstats to limit the false discovery to 1% (Supporting Figure S-5). On the basis of the statistical analysis, which takes into account the number of peptides per protein and number of transitions used for quantification, the cutoff value for FC was set to 1.5 (FC > 1.5 i.e. log2FC > 0.585) to represent significantly altered regulation.

DOI: 10.1021/acs.jproteome.5b00800
J. Proteome Res. 2016, 15, 266−279

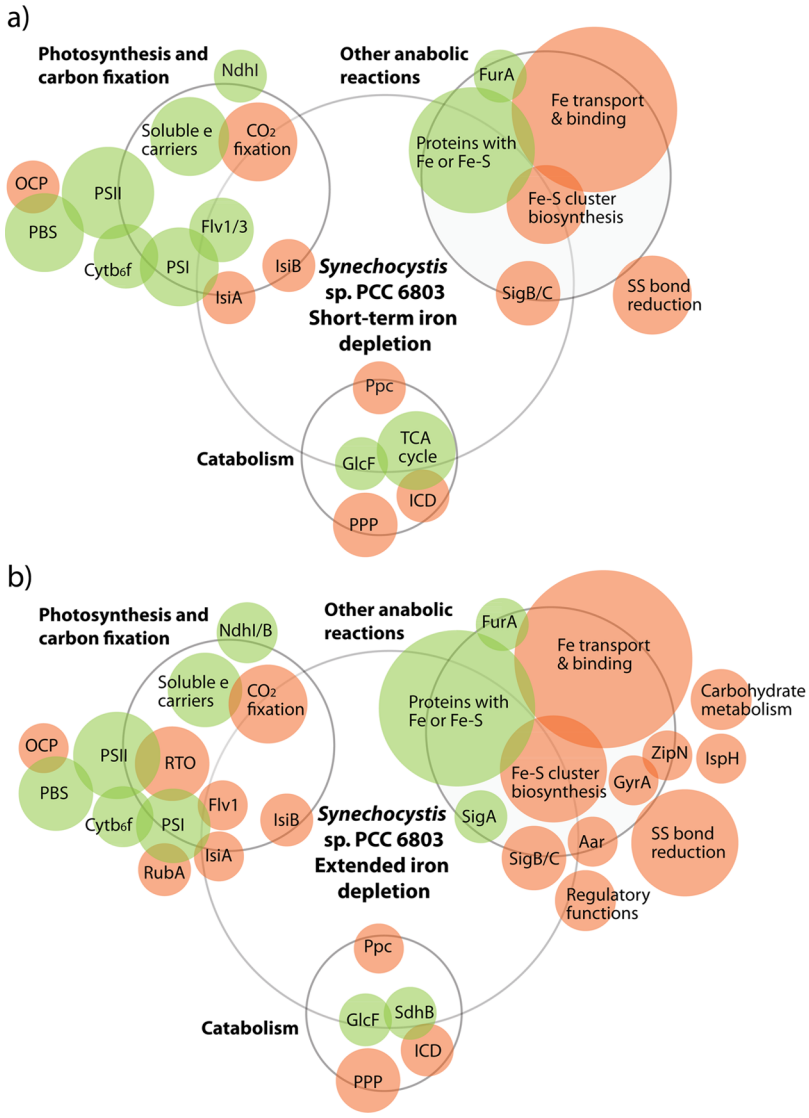

Figure 4. Simplified representation of the upregulated and downregulated target proteins (FC > 1.5) under (a) short-term iron depletion and (b) long-term iron depletion in *S.* 6803. The three functional categories (Photosynthesis and carbon fixation; Other anabolic reactions/auxiliary metabolism; Catabolism/amphibolic pathways) are represented by circles, and the upregulated and downregulated proteins as red and green balls, respectively; the size reflects the number of target proteins detected in each group. Functionally associated proteins have been grouped together into subcategories when convenient for visualization. A comprehensive listing of the protein names, annotations, descriptions, and protein expression fold changes are presented in Table 1 and S-7a (short-term iron depletion) and S-8a (long-term iron depletion). All the proteins harboring iron or an iron−sulfur cluster have been marked with * in the Tables. Abbreviations of the functional subcategories used in the figure: Cytochrome b6f complex (Cytb6f), electron (e-), iron−sulfur (Fe−S), phycobilisome (PBS), pentose phosphate pathway (PPP), photosystem (PS), respiratory terminal oxidases (RTO), disulfide (SS), tricarboxylic acid (TCA).

Under short-term iron deprivation, the observed change in the expression level of 87 proteins was statistically significant (Supporting Table S-7a), out of which 57 exceeded the abundance threshold where 29 proteins were downregulated and 28 upregulated. In comparison, 92 proteins were differentially expressed in response to extended iron deprivation (Supporting Table S-8a), out of which 71 exceeded the abundance threshold were 28 proteins were downregulated and 43 upregulated. These changes within each metabolic category have been visualized in Figure 4 and are discussed in detail below.

Photosynthesis and Carbon Fixation. In response to short-term iron deficiency of the *S.* 6803 cells, 18 out of the 33 proteins designed to represent photosynthesis and carbon fixation (listed in Supporting Table S-7b) were downregulated, and six proteins were upregulated. Clearly, downregulated proteins included soluble electron carriers such as ferredoxins (sll1382 and slr0150) and flavodiiron proteins Flv1 (sll1521) and Flv3 (sll0550). Pyruvate flavodoxin oxidoreductase (sll0741) was the most downregulated protein in this category with a 13-fold decrease in the expression level in comparison to iron-sufficient conditions. In addition, several proteins of photosynthetic complexes, like slr0342 and sll1316 of the Cytochrome b_6f complex ($Cytb_6f$); slr0737, slr1835, and ssl0563 of PSI; sll0849, ssr3451, slr1311, and sll0427 of PSII; and sll1578, slr2067 and slr0335 of the phycobilisomes (PBS) were systematically downregulated. The most upregulated proteins in this category were the typical iron stress indicators IsiA and IsiB with the highest observed expression fold-change values of 2578 and 1355, respectively. The expression of

DOI: 10.1021/acs.jproteome.5b00800
J. Proteome Res. 2016, 15, 266−279

proteins associated with CO_2 fixation (sll1031, sll1734, slr0009) was also enhanced under iron insufficiency. The orange carotenoid protein (OCP; slr1963), which interacts with phycobilisomes (PBS) and is involved in the photoprotection was also upregulated.

In response to long-term iron deprivation, out of the 35 targeted proteins associated with photosynthesis and carbon fixation, 17 proteins demonstrated significant downregulation, and 11 proteins were upregulated (Supporting Table S-8b). The overall expression trends were very similar as observed upon short-term iron deprivation (at $OD_{750\ nm} \sim 1$), with the exception of Flv1 which was upregulated in the long term experiment. In analogy, Flv3 was also upregulated but below the abundance threshold. Under the long-term iron deprivation many of the proteins had more pronounced expression fold changes than in the shorter treatment. These proteins included fructose-1,6-/sedoheptulose-1,7-bisphosphatase (slr2094), the PSI biogenesis related protein rubredoxin, RubA (slr2033), and respiratory terminal oxidases (RTO) (slr2082, sll0813, slr1379).

Other Anabolic Reactions/Auxiliary Metabolism. Under short and extended iron deprivation, the SRM analysis revealed statistically significant expression changes altogether in 45 and 47 target proteins from the category "other anabolic reactions/auxiliary metabolism", respectively. The short-term treatment resulted in an increase of the expression level of seven proteins and a decrease of 18 proteins (Supporting Table S-7c). In comparison, nine proteins in this category were significantly downregulated, and as many as 28 proteins were upregulated in the prolonged cultivation (Supporting Table S-8c).

The most extensively downregulated proteins contained iron as a cofactor, such as diaphorase subunits of bidirectional hydrogenase (sll1221, sll1223) and superoxide dismutase (slr1516). In addition, the ferric uptake regulation protein, FurA (sll0567), which is the repressor of the most upregulated iron homeostasis responsive proteins under iron deprivation,[57] was significantly down. Under prolonged iron stress, the expression levels of the hydrogenase subunit of the bidirectional hydrogenase, HoxH (sll1226) and the RNA polymerase sigma factor SigA (slr0653) were also markedly reduced.

The most upregulated proteins under the short-term iron deprivation were associated with iron transport, such as the Fut proteins (slr0327, sll1878, slr0513, slr1295) and other iron stress induced proteins like MrgA (slr1894), FeoB (slr1392), and FhuA (sll1406). The expression levels of the sigma factors SigB (sll0306) and SigC (sll0184) were also clearly higher in comparison to the normal conditions. In addition, SufR (sll0088), the transcriptional repressor of the operon responsible for biogenesis of iron−sulfur clusters, as well as the cysteine desulfurase NifS (slr0387) and L-cysteine/cystine lyase (slr2143) which are likely involved in the mobilization of sulfur into the [Fe−S] clusters[58] were upregulated. The expression of proteins involved in thiol group reduction (sll1621, slr1562, slr0600) was also induced by iron deprivation. DNA gyrase (slr0417) responsible for DNA unwinding, acyl-ACP reductase (sll0209) taking part in hydrocarbon biosynthesis and 1,4-alpha-glucan branching enzyme (sll0158) of the sugar metabolism were also upregulated.

Under long-term iron deprivation, the observed changes in protein expression were rather extensive, and many of the upregulated proteins were the same as in the short term treatment but at higher amplitude. The protein targets with significantly increased expression included thioredoxins (slr0623, slr1139), proteins with regulatory functions such as LexA (sll1626) and NtcA (sll1423), and GlgP (sll1356), related to carbohydrate storage. The expression of the iron−sulfur cluster biosynthesis associated proteins SufD (slr0076) and SufS (slr0077) was also increased. In addition, the intracellular level of the cell division protein ZipN (sll0169), which takes part in the assembly of the cyanobacterial divisome,[59] was significantly higher than in the other conditions.

Catabolism/Amphibolic Pathways. Out of the 10 targets associated with catabolism and related amphibolic pathways (Supporting Table S-7d) all the significantly downregulated proteins contained iron−sulfur clusters and were associated with the TCA cycle (slr0665, sll0823, and sll1625) or the glycolate cycle (sll1831). On the contrary, proteins with over 1.5-fold increase in expression were phosphoenolpyruvate carboxylase (sll0920) and enzymes in the pentose phosphate pathway (slr1843 and sll0329), which divert the flux away from the TCA cycle and glycolysis, respectively. The observed effects were similar in short and long-term iron deprivation although more profound at the latter time point (Supporting Table S-8d).

DISCUSSION

Demand for Quantitative Proteomics for Cyanobacteria (*S.* 6803)

Synechocystis sp. PCC 6803 is one of the most extensively studied cyanobacterial model species, with an established status particularly in photosynthesis research, and with prospects to be used as an engineered biocatalyst in future biotechnology. As the information on integration of different cellular processes has expanded due to the application of various transcriptomics methods together with extensive metabolic modeling and more directed biochemical approaches, the need for reliable and comprehensive proteomics methods to provide complementary information also on the protein level has increased. This is particularly important in view of recent observations implicating that the environmental or mutation induced changes on transcript level are frequently realized in the opposite way on the protein level.[17,60] Thus, the elucidation of the regulatory networks of any metabolic pathway requires thorough analysis at all omics levels. In this paper, we demonstrate the development and validation of SRM assays for *S.* 6803. Altogether 106 proteins were targeted on the basis of their central role in metabolic subsystems under study and the target proteins were categorized into three central metabolic groups (1) photosynthesis and carbon fixation, (2) other anabolic reactions/auxiliary metabolism, and (3) catabolism/amphibolic pathways. The SRM method allowed us to conduct a sensitive and high throughput case study to assess dynamic changes in different metabolic pathways of *S.* 6803 upon growth with differing iron-availability.

S. 6803 SRM-Assay Setup and Data-Analysis

The establishment of a reliable SRM-method for any protein is dependent on several important parameters that need to be verified and optimized.[21] These guidelines were also followed here in building the SRM protocol for *S.* 6803. First of all, there is a requirement for sufficient number of PTPs, two at a minimum, to represent the targeted protein. Second, in order to exclude the interfering signals, one PTP should be characterized by at least three coeluting transitions with

DOI: 10.1021/acs.jproteome.5b00800
J. Proteome Res. 2016, 15, 266−279

Gaussian peak shape. Additional verification of the peptide identity is based on spectral dot product score,[61] which compares the similarity of the relative fragment ion intensities of the reference spectra with the corresponding SRM transitions. However, because the peptide fragmentation patterns vary between mass spectrometers due to different activation modes (HCD or CID) or collision energies applied, the dot values cannot be considered as an ultimate basis for the peptide identification. Furthermore, the retention time correlation between the predicted (SSRCalc) or empirical (iRT) and the actual peptide retention time can be used for identity verification.

The scope of proteins selected for the *S.* 6803 SRM assay was limited by the strict criteria for PTPs. Some proteins of interest that were detected in the DDA were not targeted in SRM because of the lack of a sufficient number of PTPs (Supporting Table S-9). This is typical for proteins with small molecular mass, which restrains the total number of available peptides. For example, the 39 aa long PsaJ (sml0008) and 70 aa long HliC (ssl1633) were all represented by only one qualified PTP, whereas for the 39 aa long PsbJ (smr0008), the 40 aa long PsaI (smr0004) and 47 aa long HliB (ssr2595) no qualified PTPs were available. Proteins which were left out from the SRM-analysis due to lack of PTPs also included the 75 aa long [4Fe-4S] type iron−sulfur protein (PetF; ssr3184), 76 aa long assembly factor for iron−sulfur clusters (NifU; ssl2667) and 86 aa long PsaK (ssr0390), but also larger proteins such as PsaL (slr1655) with 157 aa and HoxY (sll1224) with 182 aa. For plastocyanin (sll0199) there are two PTPs, but only one was detectable in our study, hence also plastocyanin was left out from the analysis.

Synthetic peptides were used to expand the scope of the method to include also the proteins which were not reliably detected by DDA and to increase the coverage for the SRM assay for *S.* 6803. The synthetized PTPs were used for 22 proteins with poor or without any fragmentation spectra in DDA and 24 target proteins with insufficient number of detected endogenous peptides (minimum of two) in the shotgun approach. The MS/MS spectra from synthetized peptides allowed developing SRM assays for altogether 46 proteins more than would have been possible based only on the primary DDA data (Supporting Table S-1).

Although the lack of PTPs can prevent the development of the assays for some proteins, the strict requirements for the peptides used in SRM are typically the price to pay for the high quality of quantitative data. The constraints applied here allow confident peptide identification and reliable quantification leading to a minimum number of false positives.

There are, however, issues that can weaken the performance of an SRM-experiment and result in problems in data quality. To enable an easy and straightforward SRM-protocol at high throughput, we used a label-free approach and unfractionated cell lysates of *S.* 6803 to avoid additional sample processing steps. With this protocol, the emphasis is on careful sample preparation as well as on stable performance of the mass spectrometer. Although the SRM-method is highly sensitive due to the narrow data acquisition window for each peptide and two-stage filtering of the selected transitions in QQQ-MS, there is still a chance of interfering unspecific signals arising from the complex sample background. In the presented data set the SRM traces were evaluated by *peak scoring model* -algorithm implemented in mProphet, which allowed the minimization of the influence of interferences in the final results (Supporting Information). Prefractionation and/or enrichment of the sample may be used to increase the sensitivity for peptide detection, but the drawbacks of such additional sample processing steps are less precise measurements.[62] Furthermore, it has been reported that the sensitivity for detecting the SRM-signals can be increased by using collision energy optimization for each transition.[63] However, the optimization is required only when particularly high sensitivity is needed, and usually the predicted collision energies for each peptide is sufficient for good sensitivity.[62]

The extent, design and aims of the experiment are important when considering a statistical model for the data-analysis. The determination of the extent of the conclusion from the experiment depends on the amount of biological replicates used in the study. Our *S.* 6803 case study included three replicates, and the scope of biological replication was determined as *restricted*. The applied algorithm takes into account the measurement errors, but does not include the biological variation as the sample size does not adequately represent the underlying population.[64] Although this might result in false positives in the statistical analysis (i.e., low *p*-values), the restricted scope of conclusions was considered adequate for the current study as the aim was to screen the overall changes in a subset of the *S.* 6803 proteome rather than to validate the absolute expression changes (as in many clinical studies). Random and protein-independent distribution of the target peptides into three transition lists enabled the creation of an unbiased experimental setup where peptides of the same protein could be detected in either one, two, or three different runs. The peptide distribution into three different methods is shown in Supporting Table S-1.

Evaluation of the SRM-Method in Proteomics Analysis of *S.6803*

Technical Comparison. The most extensive proteomics study carried out so far with *S.* 6803 was conducted by Wegener et al. 2010.[17] They tested altogether 33 different environmental conditions, including iron deprivation, and analyzed the samples with a label-free shotgun LC-MS/MS method. As the scope, aim, and the method itself in SRM and LC-MS/MS analyses are very different, the comparison between these two methods is not straightforward. However, both studies provided protein expression data from *S.* 6803 under iron deprivation, making it possible to compare the overall trends in protein expression profiles between the shotgun and SRM analysis, despite the differing sampling time and setup (24 h vs $OD_{750\ nm}$∼ 1.0 in iron depletion).

Out of the 392 proteins quantified in the shotgun analysis,[17] 32 proteins were also targeted for quantification in our SRM study. Importantly, our SRM analysis gave information about the abundancy of 64 proteins which could not be quantified with the LC-MS/MS method under similar experimental conditions. Despite the smaller number of target proteins in comparison to the shotgun method, the SRM approach was superior to the shotgun method with respect to enabling the quantification of a relatively large number of low-abundance proteins. This enabled detailed information on proteins associated with specific and selected metabolic events, which remained undiscovered by the other study. It should also be emphasized that despite the use of sample fractionation in order to increase proteome coverage, the LC-MS/MS analysis missed many membrane proteins quantified in the unfractionated samples by SRM (see MPs with a gray background in

DOI: 10.1021/acs.jproteome.5b00800
J. Proteome Res. 2016, 15, 266−279

Table 1). In conclusion, the two quantitative proteomics methods clearly complement one another in revealing a comprehensive overall picture as well as a much more precise blueprint of metabolic changes that take place within the cell.

Biological Comparison. Although the experimental setup of the iron deprivation experiment in our SRM study was different from the proteomic study of Wegener et al.,[17] expression changes were similar for 25 out of the 32 proteins quantified in both studies, while seven proteins showed opposite expression trends. Of the differentially expressed proteins, three were down-regulated in SRM but upregulated in LC-MS/MS. These proteins comprised the phycobilisome subunits CpcA (sll1578) and ApcA (slr2067) as well as the PSII manganese stabilizing polypeptide PsbO (sll0427). Conversely, GcpE (slr2136), ZipN (sll0169), CydA (slr1379), and IcdA (slr1289) were upregulated in SRM, but downregulated in LC-MS/MS -analysis.

Comparison of the SRM data (Table 1) with transcriptomics data from three different microarray experiments,[65−67] revealed clear differences between gene and protein expression (see the comparisons in Supporting Table S-10). This may reflect differences in translational efficiency from individual transcripts and associated regulation, including variation in the ribosome binding sites and the complex regulatory systems involving noncoding RNAs.[68] The observed differences, however, can only be explained by these factors when the transcript levels are upregulated, while the respective protein levels are down-regulated (*sigA, fed7*). The opposite phenomenon may be related to mRNA instability and high translational efficiency, together with differences in experimental setup including culture conditions and sample processing. An example of this trend is the systematic downregulation of carbon fixation related genes (*ccmM, cupA, rbcL*) and upregulation of the respective proteins upon iron deprivation, but the mechanistic details remain unknown.

SRM Analysis upon Iron Deprivation of *S.* 6803. In addition to the validation of the developed SRM assays, the case study provided new insights into protein-level changes which take place in response to iron deprivation in *S.* 6803. The selected targets were considered as key representatives of the studied subsystems and indicators of the related functions and therefore considered to provide new and comprehensive information about the metabolic contexts of interest without the need to target all the associated proteins. This was the first time SRM was applied in the study of the *S.* 6803 proteome, and as such, the method established here provides an important platform for more extensive use of SRM-based analysis of this cyanobacterial model species in the future.

The function and regulation of proteins which require iron as a catalytic cofactor is expected to be affected by the availability of iron inside the cell. Indeed, a direct correlation between iron deprivation and downregulation of enzymes containing iron such as soluble electron carriers and those associated with photosynthetic complexes was clearly demonstrated (Table 1 and Figure 4a,b). In parallel, the enzymes involved in iron and sulfur mobilization and acquisition as well as in [Fe−S] cluster biosynthesis were upregulated in response to insufficient availability of iron. Likewise, the expression of thioredoxins was enhanced by iron deprivation, which is consistent with their proposed function as regulators of the ferric uptake regulator (FurA) and aconitate hydrase B (AcnB), which both affect the transcription of genes related to iron metabolism.[69] As thioredoxins are key regulators of enzymes in carbon assimilation,[70] along with many other functions, the upregulation of the three Calvin cycle proteins targeted in our SRM (Sll1525, Slr2094, and Slr0009) may also represent one of the metabolic interconnections induced by iron deprivation.

Not only the enzymes in carbon fixation but also other proteins that function as electron sinks, such as terminal respiratory oxidases and flavodiiron (Flv1 and Flv3) proteins were upregulated at different points in response to iron deprivation. This may reflect an imbalance between photosynthetic electron flow and the utilization of reducing equivalents for metabolism under iron deprived conditions. As a compensatory mechanism, in order to alleviate the over-reduction of the photosynthetic electron transport chain, cyanobacteria typically regulate the expression of the Flv proteins.[71,72] Flv 1 and Flv3 proteins have a lactamase domain containing a di-iron center. It is conceivable that in the beginning of iron stress, a general response is that all molecules containing iron are down-regulated. However, upon acclimation to iron stress a new homeostasis is reached that favors the expression of the Flv1 and Flv3 proteins as crucial dissipaters of excess electrons that otherwise would damage the PSI centers.[72] Indeed, both Flv1 and Flv3 are upregulated under long-term iron deprivation, despite the fact that Flv3 remains below the 1.5-fold-change threshold level.

At the same time, a decreased amount of the light-harvesting phycobiliproteins reduce the excitation pressure at the reaction centers, while the increased expression of the phycobilisome-associated orange carotenoid protein (ocp) promotes the dissipation of excess energy as heat.[73,74] In addition to these mechanisms, iron stress induces high accumulation of IsiA protein[75] (Table 1) which functions in photoprotection against excess light energy. IsiA is highly accumulated around PSI under iron depletion,[76,77] but it can also self-aggregate in prolonged iron stress to enhance the thermal dissipation and protection of the cells from photo-oxidative stress.[78,79]

Concerning the enzymes taking part in catabolism, the changes observed in protein expression suggest that under iron deprivation the metabolic flux is diverted away from the TCA cycle, while the pentose phosphate pathway is favored. These changes may be initiated by the presumed damage of PSI centers that are in danger upon iron deprivation, which in turn is expected to result in a scarcity of NADPH, the reduced cofactor that is important for anabolism. This is in agreement with the upregulation (even though subtle) of the membrane-bound transhydrogenase PntA (slr1239), which is likely to be associated with the maintenance of the intracellular NADH/NADPH balance. On the other hand, the changes in the expression profile may in part be linked directly with compromised function of the iron containing enzymes in the TCA cycle under the iron limitation.

■ CONCLUSION

In conclusion, the validated SRM method for *S.* 6803 will provide new opportunities for systems biology analysis of metabolic processes in cyanobacteria, both for the study of natural systems as well as engineered strains to be used for applications. Although the presented method does not allow the coverage achieved by the DDA approach, it does generate more consistent and precise data. SRM assays can be potentially used to replace the traditional antibody-based protein detection methods, as it may provide information on a similar level of sensitivity, but with improved quantitative measures. The validated SRM assay parameters presented in

DOI: 10.1021/acs.jproteome.5b00800
J. Proteome Res. 2016, 15, 266−279

this paper can now be used universally and they are deposited in public repositories (PeptideAtlas and Panorama Public).

■ ASSOCIATED CONTENT

Supporting Information

The Supporting Information is available free of charge on the ACS Publications website at DOI: 10.1021/acs.jproteome.5b00800.

Links to the results in public databases: Panorama Public-Skyline files with SRM results: https://panoramaweb.org/labkey/Vuorijoki_et_al_2015.url; PASSEL data set including transition list and raw files: https://db.systemsbiology.net/sbeams/cgi/PeptideAtlas/PASS_View ; PASS00726 growth of *Synechocystis* sp. PCC 6803 under iron deprivation; *in vivo* absorbance spectrum of *S.* 6803 under iron deprivation; standard curve for iRT-peptides in the alignment run; coefficient of variation of every peptide for 3 biological replicates of WT under standard condition; estimation of significance of the expression level change (FC) in the experiment (PDF)

Endogenous and synthetic peptides used in the SRM-assay; MSstats input file; identification of proteins and corresponding peptides in DDA; coefficient of variation calculated for every peptide and each condition for 3 biological replicates; Fe-depletion at $OD_{750\ nm}$ ∼ 1 vs standard conditions at $OD_{750\ nm}$ ∼ 1; extended 12-d Fe-depletion vs std conditions at $OD_{750\ nm}$ ∼ 1; FC for statistically significant proteins: Fe-depletion vs std conditions; FC for statistically significant proteins: extended 12-d Fe-depletion vs std conditions; examples of nonquantifiable proteins in *S.* 6803; SRM-study vs shotgun proteomics and transcriptomics (XLSX)

R-code applied in data-analysis (TXT)

■ AUTHOR INFORMATION

Corresponding Author

*E-mail: dokrmu@utu.fi. Phone: +358 2 333 8071.

Notes

The authors declare no competing financial interest.

■ ACKNOWLEDGMENTS

This work was financially supported by the Academy of Finland [grant no. 253269 to P.J. and P.K. and grant nos. 272424, 271832, and 273870 to EMA] and Tekes [grant no. 40128/14 to EMA]. The Biocenter Finland and the Proteomics Facility of the Turku Centre for Biotechnology are thanked for the support.

■ REFERENCES

(1) Carpenter, E. J.; Romans, K. Major role of the cyanobacterium trichodesmium in nutrient cycling in the north atlantic ocean. *Science* **1991**, *254* (5036), 1356−8.

(2) Nabout, J.; da Silva Rocha, B.; Carneiro, F.; Sant'Anna, C. How many species of Cyanobacteria are there? Using a discovery curve to predict the species number. *Biodiversity and Conservation* **2013**, *22* (12), 2907−2918.

(3) Gudmundsson, S.; Nogales, J. Cyanobacteria as photosynthetic biocatalysts: a systems biology perspective. *Mol. BioSyst.* **2015**, *11* (1), 60−70.

(4) Batth, T. S.; Singh, P.; Ramakrishnan, V. R.; Sousa, M. M.; Chan, L. J.; Tran, H. M.; Luning, E. G.; Pan, E. H.; Vuu, K. M.; Keasling, J. D.; Adams, P. D.; Petzold, C. J. A targeted proteomics toolkit for high-throughput absolute quantification of Escherichia coli proteins. *Metab. Eng.* **2014**, *26*, 48−56.

(5) Chong, P. K.; Gan, C. S.; Pham, T. K.; Wright, P. C. Isobaric tags for relative and absolute quantitation (iTRAQ) reproducibility: Implication of multiple injections. *J. Proteome Res.* **2006**, *5* (5), 1232−40.

(6) Gan, C. S.; Chong, P. K.; Pham, T. K.; Wright, P. C. Technical, experimental, and biological variations in isobaric tags for relative and absolute quantitation (iTRAQ). *J. Proteome Res.* **2007**, *6* (2), 821−7.

(7) Unlü, M.; Morgan, M. E.; Minden, J. S. Difference gel electrophoresis: a single gel method for detecting changes in protein extracts. *Electrophoresis* **1997**, *18* (11), 2071−7.

(8) Slabas, A. R.; Suzuki, I.; Murata, N.; Simon, W. J.; Hall, J. J. Proteomic analysis of the heat shock response in Synechocystis PCC6803 and a thermally tolerant knockout strain lacking the histidine kinase 34 gene. *Proteomics* **2006**, *6* (3), 845−64.

(9) Li, T.; Yang, H. M.; Cui, S. X.; Suzuki, I.; Zhang, L. F.; Li, L.; Bo, T. T.; Wang, J.; Murata, N.; Huang, F. Proteomic study of the impact of Hik33 mutation in Synechocystis sp. PCC 6803 under normal and salt stress conditions. *J. Proteome Res.* **2012**, *11* (1), 502−14.

(10) Thompson, A.; Schäfer, J.; Kuhn, K.; Kienle, S.; Schwarz, J.; Schmidt, G.; Neumann, T.; Johnstone, R.; Mohammed, A. K.; Hamon, C. Tandem mass tags: a novel quantification strategy for comparative analysis of complex protein mixtures by MS/MS. *Anal. Chem.* **2003**, *75* (8), 1895−1904.

(11) Guo, J.; Nguyen, A. Y.; Dai, Z.; Su, D.; Gaffrey, M. J.; Moore, R. J.; Jacobs, J. M.; Monroe, M. E.; Smith, R. D.; Koppenaal, D. W.; Pakrasi, H. B.; Qian, W. J. Proteome-wide light/dark modulation of thiol oxidation in cyanobacteria revealed by quantitative site-specific redox proteomics. *Mol. Cell. Proteomics* **2014**, *13* (12), 3270−85.

(12) Ross, P. L.; Huang, Y. N.; Marchese, J. N.; Williamson, B.; Parker, K.; Hattan, S.; Khainovski, N.; Pillai, S.; Dey, S.; Daniels, S.; Purkayastha, S.; Juhasz, P.; Martin, S.; Bartlet-Jones, M.; He, F.; Jacobson, A.; Pappin, D. J. Multiplexed protein quantitation in Saccharomyces cerevisiae using amine-reactive isobaric tagging reagents. *Mol. Cell. Proteomics* **2004**, *3* (12), 1154−1169.

(13) Battchikova, N.; Vainonen, J. P.; Vorontsova, N.; Keranen, M.; Carmel, D.; Aro, E. M. Dynamic changes in the proteome of Synechocystis 6803 in response to CO(2) limitation revealed by quantitative proteomics. *J. Proteome Res.* **2010**, *9* (11), 5896−912.

(14) Rowland, J. G.; Simon, W. J.; Nishiyama, Y.; Slabas, A. R. Differential proteomic analysis using iTRAQ reveals changes in thylakoids associated with Photosystem II-acquired thermotolerance in Synechocystis sp. PCC 6803. *Proteomics* **2010**, *10* (10), 1917−29.

(15) Spät, P.; Maček, B.; Forchhammer, K. Phosphoproteome of the cyanobacterium Synechocystis sp. PCC 6803 and its dynamics during nitrogen starvation. *Front. Microbiol.* **2015**, *6*, 248.

(16) Liu, H.; Sadygov, R. G.; Yates, J. R. A model for random sampling and estimation of relative protein abundance in shotgun proteomics. *Anal. Chem.* **2004**, *76* (14), 4193−201.

(17) Wegener, K. M.; Singh, A. K.; Jacobs, J. M.; Elvitigala, T.; Welsh, E. A.; Keren, N.; Gritsenko, M. A.; Ghosh, B. K.; Camp, D. G.; Smith, R. D.; Pakrasi, H. B. Global proteomics reveal an atypical strategy for carbon/nitrogen assimilation by a cyanobacterium under diverse environmental perturbations. *Mol. Cell. Proteomics* **2010**, *9* (12), 2678−89.

(18) Chelius, D.; Bondarenko, P. V. Quantitative profiling of proteins in complex mixtures using liquid chromatography and mass spectrometry. *J. Proteome Res.* **2002**, *1* (4), 317−23.

(19) Talamantes, T.; Ughy, B.; Domonkos, I.; Kis, M.; Gombos, Z.; Prokai, L. Label-free LC-MS/MS identification of phosphatidylglycerol-regulated proteins in Synechocystis sp. PCC6803. *Proteomics* **2014**, *14* (9), 1053−7.

(20) Battchikova, N.; Angeleri, M.; Aro, E. M. Proteomic approaches in research of cyanobacterial photosynthesis. *Photosynth. Res.* **2015**, *126*, 47.

DOI: 10.1021/acs.jproteome.5b00800
J. Proteome Res. 2016, 15, 266−279

(21) Lange, V.; Picotti, P.; Domon, B.; Aebersold, R. Selected reaction monitoring for quantitative proteomics: a tutorial. *Mol. Syst. Biol.* **2008**, *4*, 222.
(22) Röst, H. L.; Malmström, L.; Aebersold, R. Reproducible quantitative proteotype data matrices for systems biology. *Mol. Biol. Cell* **2015**, *26* (22), 3926−31.
(23) Gong, Y.; Li, X.; Yang, B.; Ying, W.; Li, D.; Zhang, Y.; Dai, S.; Cai, Y.; Wang, J.; He, F.; Qian, X. Different immunoaffinity fractionation strategies to characterize the human plasma proteome. *J. Proteome Res.* **2006**, *5* (6), 1379−87.
(24) Tu, C.; Rudnick, P. A.; Martinez, M. Y.; Cheek, K. L.; Stein, S. E.; Slebos, R. J.; Liebler, D. C. Depletion of abundant plasma proteins and limitations of plasma proteomics. *J. Proteome Res.* **2010**, *9* (10), 4982−91.
(25) Whiteaker, J. R.; Zhang, H.; Eng, J. K.; Fang, R.; Piening, B. D.; Feng, L. C.; Lorentzen, T. D.; Schoenherr, R. M.; Keane, J. F.; Holzman, T.; Fitzgibbon, M.; Lin, C.; Cooke, K.; Liu, T.; Camp, D. G.; Anderson, L.; Watts, J.; Smith, R. D.; McIntosh, M. W.; Paulovich, A. G. Head-to-head comparison of serum fractionation techniques. *J. Proteome Res.* **2007**, *6* (2), 828−836.
(26) Anderson, L.; Hunter, C. L. Quantitative mass spectrometric multiple reaction monitoring assays for major plasma proteins. *Mol. Cell. Proteomics* **2005**, *5* (4), 573−588.
(27) Kuster, B.; Schirle, M.; Mallick, P.; Aebersold, R. Scoring proteomes with proteotypic peptide probes. *Nat. Rev. Mol. Cell Biol.* **2005**, *6* (7), 577−83.
(28) Abbatiello, S. E.; Schilling, B.; Mani, D. R.; Zimmerman, L. J.; Hall, S. C.; MacLean, B.; Albertolle, M.; Allen, S.; Burgess, M.; Cusack, M. P.; Gosh, M.; Hedrick, V.; Held, J. M.; Inerowicz, H. D.; Jackson, A.; Keshishian, H.; Kinsinger, C. R.; Lyssand, J.; Makowski, L.; Mesri, M.; Rodriguez, H.; Rudnick, P.; Sadowski, P.; Sedransk, N.; Shaddox, K.; Skates, S. J.; Kuhn, E.; Smith, D.; Whiteaker, J. R.; Whitwell, C.; Zhang, S.; Borchers, C. H.; Fisher, S. J.; Gibson, B. W.; Liebler, D. C.; MacCoss, M. J.; Neubert, T. A.; Paulovich, A. G.; Regnier, F. E.; Tempst, P.; Carr, S. A. Large-Scale Interlaboratory Study to Develop, Analytically Validate and Apply Highly Multiplexed, Quantitative Peptide Assays to Measure Cancer-Relevant Proteins in Plasma. *Mol. Cell. Proteomics* **2015**, *14* (9), 2357−74.
(29) Aebersold, R.; Burlingame, A. L.; Bradshaw, R. A. Western blots versus selected reaction monitoring assays: time to turn the tables? *Mol. Cell. Proteomics* **2013**, *12* (9), 2381−2.
(30) Picotti, P.; Bodenmiller, B.; Mueller, L. N.; Domon, B.; Aebersold, R. Full dynamic range proteome analysis of S. cerevisiae by targeted proteomics. *Cell* **2009**, *138* (4), 795−806.
(31) Schubert, O. T.; Mouritsen, J.; Ludwig, C.; Röst, H. L.; Rosenberger, G.; Arthur, P. K.; Claassen, M.; Campbell, D. S.; Sun, Z.; Farrah, T.; Gengenbacher, M.; Maiolica, A.; Kaufmann, S. H.; Moritz, R. L.; Aebersold, R. The Mtb proteome library: a resource of assays to quantify the complete proteome of Mycobacterium tuberculosis. *Cell Host Microbe* **2013**, *13* (5), 602−12.
(32) Hüttenhain, R.; Soste, M.; Selevsek, N.; Röst, H.; Sethi, A.; Carapito, C.; Farrah, T.; Deutsch, E. W.; Kusebauch, U.; Moritz, R. L.; Niméus-Malmström, E.; Rinner, O.; Aebersold, R. Reproducible quantification of cancer-associated proteins in body fluids using targeted proteomics. *Sci. Transl. Med.* **2012**, *4* (142), 142ra94.
(33) Hüttenhain, R.; Surinova, S.; Ossola, R.; Sun, Z.; Campbell, D.; Cerciello, F.; Schiess, R.; Bausch-Fluck, D.; Rosenberger, G.; Chen, J.; Rinner, O.; Kusebauch, U.; Hajdúch, M.; Moritz, R. L.; Wollscheid, B.; Aebersold, R. N-glycoprotein SRMAtlas: a resource of mass spectrometric assays for N-glycosites enabling consistent and multiplexed protein quantification for clinical applications. *Mol. Cell. Proteomics* **2013**, *12* (4), 1005−16.
(34) Liu, Y.; Hüttenhain, R.; Surinova, S.; Gillet, L. C.; Mouritsen, J.; Brunner, R.; Navarro, P.; Aebersold, R. Quantitative measurements of N-linked glycoproteins in human plasma by SWATH-MS. *Proteomics* **2013**, *13* (8), 1247−56.
(35) Konert, G.; Trotta, A.; Kouvonen, P.; Rahikainen, M.; Durian, G.; Blokhina, O.; Fagerstedt, K.; Muth, D.; Corthals, G. L.; Kangasjärvi, S. Protein phosphatase 2A (PP2A) regulatory subunit B′γ interacts with cytoplasmic ACONITASE 3 and modulates the abundance of AOX1A and AOX1D in Arabidopsis thaliana. *New Phytol.* **2015**, *205* (3), 1250−63.
(36) Taylor, N. L.; Fenske, R.; Castleden, I.; Tomaz, T.; Nelson, C. J.; Millar, A. H. Selected reaction monitoring to determine protein abundance in Arabidopsis using the Arabidopsis proteotypic predictor. *Plant Physiol.* **2014**, *164* (2), 525−36.
(37) Saito, M. A.; Bertrand, E. M.; Dutkiewicz, S.; Bulygin, V. V.; Moran, D. M.; Monteiro, F. M.; Follows, M. J.; Valois, F. W.; Waterbury, J. B. Iron conservation by reduction of metalloenzyme inventories in the marine diazotroph Crocosphaera watsonii. *Proc. Natl. Acad. Sci. U. S. A.* **2011**, *108* (6), 2184−9.
(38) Wase, N.; Pham, T. K.; Ow, S. Y.; Wright, P. C. Quantitative analysis of UV-A shock and short term stress using iTRAQ, pseudo selective reaction monitoring (pSRM) and GC-MS based metabolite analysis of the cyanobacterium Nostoc punctiforme ATCC 29133. *J. Proteomics* **2014**, *109*, 332−55.
(39) ÖQuist, G. Changes in Pigment Composition and Photosynthesis Induced by Iron-Deficiency in the Blue-Green Alga Anacystis nidulans. *Physiol. Plant.* **1971**, *25* (2), 188−191.
(40) MacLean, B.; Tomazela, D. M.; Shulman, N.; Chambers, M.; Finney, G. L.; Frewen, B.; Kern, R.; Tabb, D. L.; Liebler, D. C.; MacCoss, M. J. Skyline: an open source document editor for creating and analyzing targeted proteomics experiments. *Bioinformatics* **2010**, *26* (7), 966−8.
(41) Kaneko, T.; Sato, S.; Kotani, H.; Tanaka, A.; Asamizu, E.; Nakamura, Y.; Miyajima, N.; Hirosawa, M.; Sugiura, M.; Sasamoto, S.; Kimura, T.; Hosouchi, T.; Matsuno, A.; Muraki, A.; Nakazaki, N.; Naruo, K.; Okumura, S.; Shimpo, S.; Takeuchi, C.; Wada, T.; Watanabe, A.; Yamada, M.; Yasuda, M.; Tabata, S. Sequence analysis of the genome of the unicellular cyanobacterium Synechocystis sp. strain PCC6803. II. Sequence determination of the entire genome and assignment of potential protein-coding regions. *DNA Res.* **1996**, *3* (3), 109−36.
(42) Perkins, D. N.; Pappin, D. J.; Creasy, D. M.; Cottrell, J. S. Probability-based protein identification by searching sequence databases using mass spectrometry data. *Electrophoresis* **1999**, *20* (18), 3551−67.
(43) Käll, L.; Canterbury, J. D.; Weston, J.; Noble, W. S.; MacCoss, M. J. Semi-supervised learning for peptide identification from shotgun proteomics datasets. *Nat. Methods* **2007**, *4* (11), 923−5.
(44) Fusaro, V. A.; Mani, D. R.; Mesirov, J. P.; Carr, S. A. Prediction of high-responding peptides for targeted protein assays by mass spectrometry. *Nat. Biotechnol.* **2009**, *27* (2), 190−8.
(45) Mallick, P.; Schirle, M.; Chen, S. S.; Flory, M. R.; Lee, H.; Martin, D.; Ranish, J.; Raught, B.; Schmitt, R.; Werner, T.; Kuster, B.; Aebersold, R. Computational prediction of proteotypic peptides for quantitative proteomics. *Nat. Biotechnol.* **2007**, *25* (1), 125−31.
(46) Tang, H.; Arnold, R. J.; Alves, P.; Xun, Z.; Clemmer, D. E.; Novotny, M. V.; Reilly, J. P.; Radivojac, P. A computational approach toward label-free protein quantification using predicted peptide detectability. *Bioinformatics* **2006**, *22* (14), e481−8.
(47) Krokhin, O. V. Sequence-specific retention calculator. Algorithm for peptide retention prediction in ion-pair RP-HPLC: application to 300- and 100-A pore size C18 sorbents. *Anal. Chem.* **2006**, *78* (22), 7785−95.
(48) Escher, C.; Reiter, L.; MacLean, B.; Ossola, R.; Herzog, F.; Chilton, J.; MacCoss, M. J.; Rinner, O. Using iRT, a normalized retention time for more targeted measurement of peptides. *Proteomics* **2012**, *12* (8), 1111−21.
(49) Reiter, L.; Rinner, O.; Picotti, P.; Hüttenhain, R.; Beck, M.; Brusniak, M. Y.; Hengartner, M. O.; Aebersold, R. mProphet: automated data processing and statistical validation for large-scale SRM experiments. *Nat. Methods* **2011**, *8* (5), 430−5.
(50) Choi, M.; Chang, C.; Vitek, O. *MSstats: Protein Significance Analysis in DDA, SRM and DIA for Label-free or Label-based Proteomics Experiments*, R package version 2.6.0.; 2014.
(51) Choi, M.; Chang, C. Y.; Clough, T.; Broudy, D.; Killeen, T.; MacLean, B.; Vitek, O. MSstats: an R package for statistical analysis of

DOI: 10.1021/acs.jproteome.5b00800
J. Proteome Res. 2016, 15, 266−279

quantitative mass spectrometry-based proteomic experiments. *Bioinformatics* **2014**, *30*, 2524.
(52) de Graaf, E. L.; Altelaar, A. F.; van Breukelen, B.; Mohammed, S.; Heck, A. J. Improving SRM assay development: a global comparison between triple quadrupole, ion trap, and higher energy CID peptide fragmentation spectra. *J. Proteome Res.* **2011**, *10* (9), 4334−41.
(53) Sharma, V.; Eckels, J.; Taylor, G. K.; Shulman, N. J.; Stergachis, A. B.; Joyner, S. A.; Yan, P.; Whiteaker, J. R.; Halusa, G. N.; Schilling, B.; Gibson, B. W.; Colangelo, C. M.; Paulovich, A. G.; Carr, S. A.; Jaffe, J. D.; MacCoss, M. J.; MacLean, B. Panorama: a targeted proteomics knowledge base. *J. Proteome Res.* **2014**, *13* (9), 4205−10.
(54) Zhang, P.; Allahverdiyeva, Y.; Eisenhut, M.; Aro, E. M. Flavodiiron proteins in oxygenic photosynthetic organisms: photoprotection of photosystem II by Flv2 and Flv4 in Synechocystis sp. PCC 6803. *PLoS One* **2009**, *4* (4), e5331.
(55) Gilmore, J. M.; Washburn, M. P. Advances in shotgun proteomics and the analysis of membrane proteomes. *J. Proteomics* **2010**, *73* (11), 2078−91.
(56) Farrah, T.; Deutsch, E. W.; Kreisberg, R.; Sun, Z.; Campbell, D. S.; Mendoza, L.; Kusebauch, U.; Brusniak, M. Y.; Hüttenhain, R.; Schiess, R.; Selevsek, N.; Aebersold, R.; Moritz, R. L. PASSEL: the PeptideAtlas SRMexperiment library. *Proteomics* **2012**, *12* (8), 1170−5.
(57) Ghassemian, M.; Straus, N. A. Fur regulates the expression of iron-stress genes in the cyanobacterium Synechococcus sp. strain PCC 7942. *Microbiology* **1996**, *142*, 1469−76.
(58) Jaschkowitz, K.; Seidler, A. Role of a NifS-like protein from the cyanobacterium Synechocystis PCC 6803 in the maturation of FeS proteins. *Biochemistry* **2000**, *39* (12), 3416−23.
(59) Marbouty, M.; Saguez, C.; Cassier-Chauvat, C.; Chauvat, F. ZipN, an FtsA-like orchestrator of divisome assembly in the model cyanobacterium Synechocystis PCC6803. *Mol. Microbiol.* **2009**, *74* (2), 409−20.
(60) Huang, S.; Chen, L.; Te, R.; Qiao, J.; Wang, J.; Zhang, W. Complementary iTRAQ proteomics and RNA-seq transcriptomics reveal multiple levels of regulation in response to nitrogen starvation in Synechocystis sp. PCC 6803. *Mol. BioSyst.* **2013**, *9* (10), 2565−74.
(61) Stein, S. Estimating probabilities of correct identification from results of mass spectral library searches. *J. Am. Soc. Mass Spectrom.* **1994**, *5* (4), 316−323.
(62) Picotti, P.; Aebersold, R. Selected reaction monitoring-based proteomics: workflows, potential, pitfalls and future directions. *Nat. Methods* **2012**, *9* (6), 555−66.
(63) Wu, C.; Shi, T.; Brown, J. N.; He, J.; Gao, Y.; Fillmore, T. L.; Shukla, A. K.; Moore, R. J.; Camp, D. G.; Rodland, K. D.; Qian, W. J.; Liu, T.; Smith, R. D. Expediting SRM assay development for large-scale targeted proteomics experiments. *J. Proteome Res.* **2014**, *13* (10), 4479−87.
(64) Chang, C. Y.; Picotti, P.; Hüttenhain, R.; Heinzelmann-Schwarz, V.; Jovanovic, M.; Aebersold, R.; Vitek, O. Protein significance analysis in selected reaction monitoring (SRM) measurements. *Mol. Cell. Proteomics* **2012**, *11* (4), M111.014662.
(65) Singh, A. K.; McIntyre, L. M.; Sherman, L. A. Microarray analysis of the genome-wide response to iron deficiency and iron reconstitution in the cyanobacterium Synechocystis sp. PCC 6803. *Plant Physiol.* **2003**, *132* (4), 1825−1839.
(66) Shcolnick, S.; Summerfield, T. C.; Reytman, L.; Sherman, L. A.; Keren, N. The mechanism of iron homeostasis in the unicellular cyanobacterium synechocystis sp. PCC 6803 and its relationship to oxidative stress. *Plant Physiol.* **2009**, *150* (4), 2045−56.
(67) Hernández-Prieto, M. A.; Schön, V.; Georg, J.; Barreira, L.; Varela, J.; Hess, W. R.; Futschik, M. E. Iron deprivation in Synechocystis: inference of pathways, non-coding RNAs, and regulatory elements from comprehensive expression profiling. *G3: Genes, Genomes, Genet.* **2012**, *2* (12), 1475−95.
(68) Georg, J.; Voss, B.; Scholz, I.; Mitschke, J.; Wilde, A.; Hess, W. R. Evidence for a major role of antisense RNAs in cyanobacterial gene regulation. *Mol. Syst. Biol.* **2009**, *5*, 305.
(69) Kumar, J. K.; Tabor, S.; Richardson, C. C. Proteomic analysis of thioredoxin-targeted proteins in Escherichia coli. *Proc. Natl. Acad. Sci. U. S. A.* **2004**, *101* (11), 3759−64.
(70) Schurmann, P.; Jacquot, J. P. PLANT THIOREDOXIN SYSTEMS REVISITED. *Annu. Rev. Plant Physiol. Plant Mol. Biol.* **2000**, *51*, 371−400.
(71) Zhang, P.; Eisenhut, M.; Brandt, A. M.; Carmel, D.; Silén, H. M.; Vass, I.; Allahverdiyeva, Y.; Salminen, T. A.; Aro, E. M. Operon flv4-flv2 provides cyanobacterial photosystem II with flexibility of electron transfer. *Plant Cell* **2012**, *24* (5), 1952−71.
(72) Allahverdiyeva, Y.; Mustila, H.; Ermakova, M.; Bersanini, L.; Richaud, P.; Ajlani, G.; Battchikova, N.; Cournac, L.; Aro, E. M. Flavodiiron proteins Flv1 and Flv3 enable cyanobacterial growth and photosynthesis under fluctuating light. *Proc. Natl. Acad. Sci. U. S. A.* **2013**, *110* (10), 4111−6.
(73) Wilson, A.; Ajlani, G.; Verbavatz, J. M.; Vass, I.; Kerfeld, C. A.; Kirilovsky, D. A soluble carotenoid protein involved in phycobilisome-related energy dissipation in cyanobacteria. *Plant Cell* **2006**, *18* (4), 992−1007.
(74) Wilson, A.; Boulay, C.; Wilde, A.; Kerfeld, C. A.; Kirilovsky, D. Light-induced energy dissipation in iron-starved cyanobacteria: roles of OCP and IsiA proteins. *Plant Cell* **2007**, *19* (2), 656−72.
(75) Burnap, R. L.; Troyan, T.; Sherman, L. A. The highly abundant chlorophyll-protein complex of iron-deficient Synechococcus sp. PCC7942 (CP43′) is encoded by the isiA gene. *Plant Physiol* **1993**, *103* (3), 893−902.
(76) Bibby, T. S.; Nield, J.; Barber, J. Iron deficiency induces the formation of an antenna ring around trimeric photosystem I in cyanobacteria. *Nature* **2001**, *412* (6848), 743−5.
(77) Boekema, E. J.; Hifney, A.; Yakushevska, A. E.; Piotrowski, M.; Keegstra, W.; Berry, S.; Michel, K. P.; Pistorius, E. K.; Kruip, J. A giant chlorophyll-protein complex induced by iron deficiency in cyanobacteria. *Nature* **2001**, *412* (6848), 745−8.
(78) Yeremenko, N.; Kouril, R.; Ihalainen, J. A.; D'Haene, S.; van Oosterwijk, N.; Andrizhiyevskaya, E. G.; Keegstra, W.; Dekker, H. L.; Hagemann, M.; Boekema, E. J.; Matthijs, H. C.; Dekker, J. P. Supramolecular organization and dual function of the IsiA chlorophyll-binding protein in cyanobacteria. *Biochemistry* **2004**, *43* (32), 10308−10313.
(79) Ihalainen, J. A.; D'Haene, S.; Yeremenko, N.; van Roon, H.; Arteni, A. A.; Boekema, E. J.; van Grondelle, R.; Matthijs, H. C.; Dekker, J. P. Aggregates of the chlorophyll-binding protein IsiA (CP43′) dissipate energy in cyanobacteria. *Biochemistry* **2005**, *44* (32), 10846−10853.

DOI: 10.1021/acs.jproteome.5b00800
J. Proteome Res. 2016, 15, 266−279